PHYSICAL REVIEW B **80**, 220507(R) (2009)

Doppler shift in Andreev reflection from a moving superconducting condensate in Nb/InAs Josephson junctions

F. Rohlfing,[1] G. Tkachov,[2,*] F. Otto,[1] K. Richter,[2] D. Weiss,[1] G. Borghs,[3] and C. Strunk[1]
[1]*Institute for Experimental and Applied Physics, Universität Regensburg, D-93040 Regensburg, Germany*
[2]*Institute for Theoretical Physics, Universität Regensburg, D-93040 Regensburg, Germany*
[3]*Interuniversity Micro-Electronics Center (IMEC), Kapeldreef 75a, B-3001 Leuven, Belgium*
(Received 27 February 2009; revised manuscript received 29 July 2009; published 28 December 2009)

We study narrow ballistic Josephson weak links in a InAs quantum wells contacted by Nb electrodes and find a dramatic magnetic-field suppression of the Andreev reflection amplitude, which occurs even for in-plane field orientation with essentially no magnetic flux through the junction. Our observations demonstrate the presence of a Doppler shift in the energy of the Andreev levels, which results from diamagnetic screening currents in the hybrid Nb/InAs banks. The data for conductance, excess, and critical currents can be consistently explained in terms of the sample geometry and the McMillan energy, characterizing the transparency of the Nb/InAs interface.

DOI: 10.1103/PhysRevB.80.220507 PACS number(s): 74.45.+c

In recent years a detailed microscopic understanding of the proximity effect has emerged. There is now agreement that in highly transparent Josephson junctions formed by a metallic weak link in good contact with two superconducting (SC) banks the supercurrent is carried by Andreev bound states (ABSs).[1] These come in pairs corresponding to the opposite directions of Cooper-pair transfer mediated by multiple Andreev reflection (MAR) at the SC/metal interfaces provided that the acquired quasiparticle phase is a multiple of 2π.[2] At currents exceeding the critical current $I_C(T,B)$ MAR between the SC banks manifests itself in the current-voltage characteristics as subharmonic gap structures at voltages $eV_n=2\Delta/n$, where Δ is the SC energy gap and $n=1,2,\ldots$. At higher voltage $eV\gg 2\Delta$, $I(V)$ becomes linear with an excess current $I_{\mathrm{exc}}=I(V)-G_NV$ determined by a single Andreev reflection (AR) probability $|a(\varepsilon)|^2$ (G_N is the normal-state conductance).[3,4]

Weak links formed by a two-dimensional (2D) electron gas (2DEG) in semiconductor quantum wells[5] are of particular interest because here the ballistic transport can be studied. In very high magnetic field perpendicular to the 2DEG, theory[6] and experiments[7,8] have demonstrated Andreev transport via edge states. Indirect evidence for a strong magnetic-field effect on AR was experimentally found in antidot billiards.[9] The case of parallel field, with respect to the 2DEG, is equally intriguing: as ideally no magnetic flux threads the 2DEG, one may naively expect the Josephson current to survive up to the critical fields of the SC leads. This is not the case, but the underlying mechanism of the supercurrent suppression is still unclear. This question, also relevant for other 2D hybrid systems,[10] is among the issues this Rapid Communication focuses on.

In this Rapid Communication, Nb/InAs Josephson junctions of different width are studied in a four-terminal lead configuration within the 2DEG. This allows us to separately determine the transparencies of the InAs weak link and Nb/InAs interfaces and identify an additional energy scale in the electronic spectrum of the hybrid SC terminals. We observe a very strong suppression of both the AR probability and supercurrent in weak magnetic fields of 4 and 100 mT for perpendicular and parallel orientations, respectively. This unexpectedly rapid decay can be traced back to diamagnetic supercurrents in Nb, which break the time-reversal symmetry of Andreev reflection.

The samples were prepared from a heterostructure containing an InAs-quantum well with thickness $d_N=15$ nm and a mean free path around 3.7 μm, confined between two AlGaSb layers. The electron density was 7.8×10^{15} m^{-2}, resulting in a Fermi wavelength $\lambda_F=2\pi/k_F=28$ nm.[7] First, a constriction of width W with a four-terminal ($4t$) lead struc-

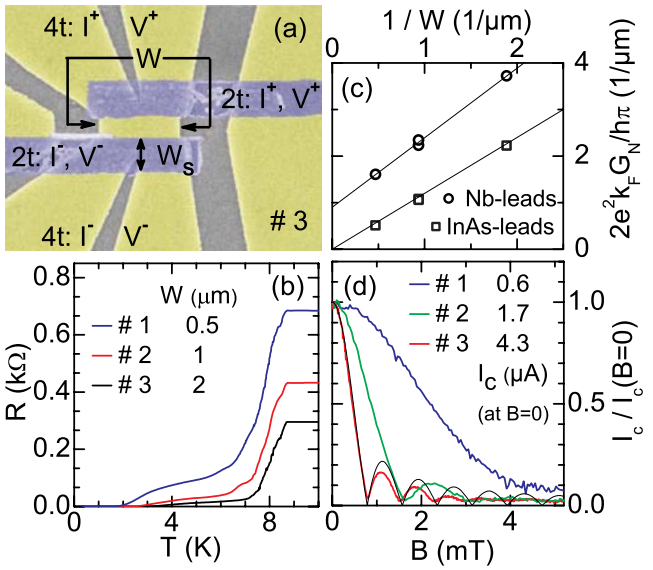

FIG. 1. (Color online) (a) Scanning electron micrograph of sample No. 3 with width $W=2$ μm and length $L=0.6$ μm. Regions with InAs two-dimensional electron gas are shown in yellow. Etched regions are light gray. The horizontal dark gray stripes are made from a 35-nm-thick Nb. (b) $R(T)$ for three samples with width $W=0.5,1,2$ μm. (c) Resistance vs $1/W$ at 10 K for the $4t$ configuration with InAs leads (○) and the $2t$ configuration with Nb leads (□). (d) Normalized supercurrent I_C vs perpendicular magnetic field $B_\perp$ for different widths W. The black curve is the standard Fraunhofer pattern fitting the data for sample No. 3 ($W=2$ μm).

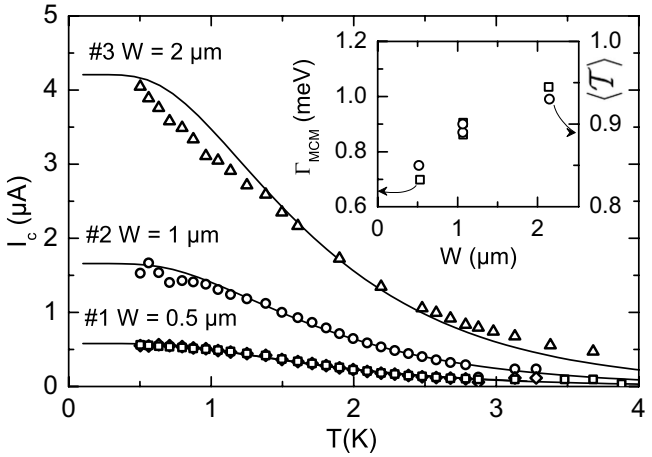

FIG. 2. Critical current vs. temperature T for different widths W together with best fits according to our model. Inset: values of $\langle \mathcal{T} \rangle$ (○) and Γ_{McM} (□) resulting from the fits.

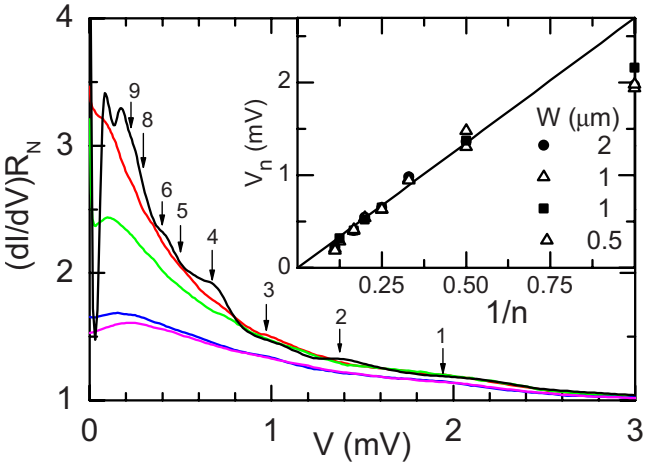

FIG. 3. (Color online) Measured differential conductance dI/dV of sample No. 2a ($W=1$ μm) for different values of a perpendicular magnetic field $B_\perp=0$, 4, 10, 40, and 100 mT, from top to bottom. Arrows indicate the subharmonic gap structure induced by multiple Andreev reflections. Inset: voltages of the subharmonic gap structures for all samples. The solid line indicates the expected slope for $\Delta_{Nb}=1.35$ meV.

ture [shown in yellow in Fig. 1(a)] was patterned using electron-beam lithograpy (EBL) and etched by reactive ion etching in a $SiCl_4$ plasma. In a second EBL step two Nb stripes were deposited onto the InAs [horizontal gray bars in Fig. 1(a)] after removal of the top AlGaSb layer and *in situ* Ar-ion cleaning of the InAs surface. The Nb stripes have a width $W_S=1$ μm and a thickness $d_S=35$ nm; their distance $L=600$ nm defines the length L of the junction. This results in a Thouless energy of $\varepsilon_{Th}=\hbar v_F/L=0.8$ meV$\lesssim\Delta$ for all samples, v_F being the Fermi velocity in the normal metal. We have prepared four samples on two chips in the same batch. The chips contained junctions with $W=0.5$ and 1 μm (denoted as No. 1 and No. 2a), and $W=1$ and 2 μm (denoted No. 2b and No. 3), respectively.

Figure 1(b) shows the two-terminal ($2t$) resistance of samples No. 1, No. 2a, and No. 3 measured through the Nb stripes vs temperature T. The resistance drops at the transition temperature of the Nb stripes around 8.3 K and again between 2 and 3 K, where the constriction becomes superconducting. In Fig. 1(c) we plot the $2t$ resistance measured across the Nb stripes and the $4t$ resistance measured within the InAs layer at $T=10$ K as a function of W. The $4t$-resistance scales as $1/W$, obeying the ballistic Landauer-Büttiker formula:

$$G_N = \frac{2e^2}{h}\sum_n \mathcal{T}_n = \frac{2e^2}{h}\frac{k_F W}{\pi}\langle \mathcal{T} \rangle, \qquad (1)$$

where $\langle \mathcal{T} \rangle$ is the average channel transparency. From the slope of $G_N(W)$ we extract $\langle \mathcal{T} \rangle=0.8$. The $2t$ resistance at 10 K is also proportional to $1/W$, however, with an offset caused by the normal-state resistance of the Nb stripes and the Nb/InAs-interface resistance. Finally, we show in Fig. 1(d) the interference pattern of the junctions in a transversal magnetic field. For the widest junction the critical current $I_C(B)$ exhibits the expected Fraunhofer pattern.[11] For the narrower ones the higher order maxima are suppressed, and in the 0.5 μm-wide device $I_C(B)$ resembles more a Gaussian rather than a Fraunhofer pattern. This will be addressed below.

Information about the spectral distribution of ABS is contained in the T dependence of the supercurrent. In Fig. 2 we present the critical current I_C at $B=0$ as a function of temperature for different widths $W=0.5$, 1, and 2 μm of the InAs constriction. With decreasing temperature $I_C(T)$ initially increases and then saturates at $T\lesssim 1$ K. The solid lines are fits based on the approach of Grajcar *et al.*[12] who adapted the scattering theory for the Josephson current[13] to 2D ballistic proximity structures. Two parameters were used in these fits: the average normal-state transmission probability $\langle \mathcal{T} \rangle$ and the McMillan energy $\Gamma_{McM}=\tau_{SN}\cdot\hbar v_F/2d_N$,[14] which is the Thouless energy of the InAs quantum well multiplied by the Nb/InAs interface transparency τ_{SN}. Γ_{McM} determines the strength of the proximity-induced superconducting correlations in the InAs regions underneath the Nb film, which act as effective superconducting terminals described by the Green's functions of the McMillan model.[12,15] Clearly, the smaller τ_{SN}, the weaker the proximity effect. Because $\langle \mathcal{T} \rangle$ influences mainly the saturation value of $I_C(T\to 0)$, while Γ_{McM} determines the decay of I_C with T, these two parameters can be extracted independently from the measured $I_C(T)$.

The fit parameters are given in the inset of Fig. 2. The values of $\langle \mathcal{T} \rangle$ scatter by $\pm 5\%$ around 0.9, which is slightly higher but still close to $\langle \mathcal{T} \rangle=0.8$ estimated independently from $4t$ resistance [Eq. (1)]. The values of Γ_{McM} scatter by $\pm 15\%$ around 0.9 meV. From this, we find $\tau_{NS}\approx 0.06$ which is much smaller than $\langle \mathcal{T} \rangle$. The high mobility of the InAs-quantum well provides the high transparency of the constriction, while the comparatively low Nb/InAs interface transparency is sufficient to transform the Nb/InAs-bilayer into an effective superconductor with the additional energy scale Γ_{McM} (see also inset in Fig. 5).

Having all sample parameters fixed, we now turn to the main topic of our study, i.e., the magnetic field dependence of Andreev reflection. First, we examine IV and dI/dV char-

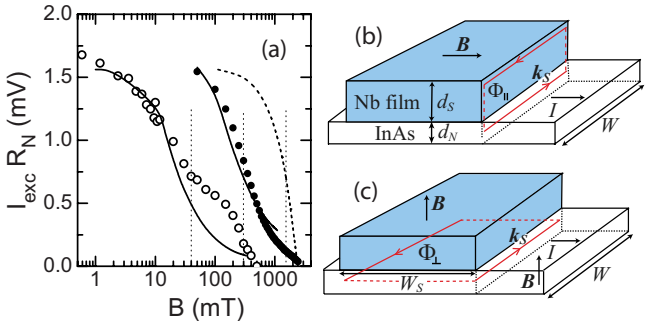

FIG. 4. (Color online) (a) Measured excess current of sample No. 2a vs perpendicular (○) and parallel (●) magnetic field. The solid lines result from our model including the Doppler shift $\varepsilon_D(k_S)$ (see text) and the dashed line shows $I_{\rm exc}$ due to the suppression of $\Delta_{Nb}(B_\parallel)$ only (Ref. 18). [(b) and (c)] One of the Nb/InAs terminals in parallel and perpendicular fields. Red arrows indicate the SC order-parameter phase gradient, $\mathbf{k}_S=\nabla\gamma$, with $k_S=-\pi/W\times\Phi/\Phi_0$ determined by the magnetic flux Φ through the bilayer for given field orientation.

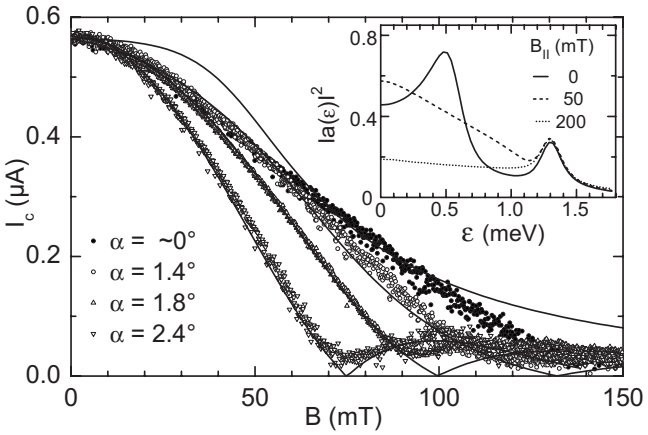

FIG. 5. Critical current vs B for sample No. 1 at small angles α between **B** and 2DEG. The lines are theoretical fits (see text). The inset shows the double peak structure of $|a(\varepsilon)|^2$ characteristic of hybrid SC and its suppression by $B_\parallel$.

acteristics. Figure 3 shows the differential conductance dI/dV of sample No. 2a ($W=1$ μm) for different values of perpendicular field $B_\perp$. At $B_\perp=0$ subharmonic gap structures (see arrows) appear at integer fractions $V_n=2\Delta_{Nb}/ne$ of $2\Delta_{Nb}$. The location of the steps vs $1/n$, plotted in the inset of Fig. 3, agrees very well with the value of $\Delta_{Nb}=1.35$ meV. The $n=1$ step appears at lower voltage as predicted in Ref. 16. A tiny perpendicular field of 4 mT washes out these features, vanishing completely at 10 mT. Also, the enhancement of dI/dV at low bias is suppressed. It is known[2,17] that the subharmonic gap structure and low bias enhancement of dI/dV originate from multiple AR at finite V. The large number of steps independently confirms the high AR probability $|a|^2$ expected from the high values of $\langle\mathcal{T}\rangle$. The rapid smearing of these steps thus indicates a surprisingly strong magnetic field dependence of $|a|^2$.

This observation is further substantiated by the behavior of the excess current $I_{\rm exc}$,[4] obtained by integrating $dI/dV-G_N$ (see Fig. 3) over voltage. Since $I_{\rm exc}$ results from a single AR at $V>2\Delta_{Nb}$, it is more robust than MAR whose amplitude is $\propto|a|^{2n}$. Figure 4 shows $I_{\rm exc}$ on a logarithmic scale for both field orientations. It is suppressed to ~50% at $B_\perp=30$ mT and $B_\parallel=300$ mT as indicated by the vertical dotted lines. The field $B_\parallel$ exceeds $B_\perp$ by an order of magnitude but is still a factor of five smaller than needed for an appreciable reduction in the gap $\Delta_{Nb}(B)$ as follows from the pair-breaking theory[18] (right dotted line in Fig. 4).

We attribute the behavior of $I_{\rm exc}(B)$ to the magnetic field suppression of the Andreev reflection at the InAs proximity regions underneath the Nb films. In the presence of the external field $\mathbf{B}=\nabla\times\mathbf{A}(\mathbf{r})$, the SC order parameter acquires an inhomogeneous phase, $\gamma(\mathbf{r})=-2\pi\Phi_0^{-1}\int_{\mathbf{r}_0}^{\mathbf{r}}\mathbf{A}(\mathbf{r}')d\mathbf{r}'$, whose gradient $\mathbf{k}_S=\nabla\gamma$ induces diamagnetic currents in the entire Nb/InAs structure, including the InAs proximity layer [see, Figs. 4(b) and 4(c)]. If $\mathbf{k}_i$ and $\mathbf{k}_f$ denote the wave vectors of initial and final quasiparticle states in the AR-process momentum conservation requires $\mathbf{k}_i+\mathbf{k}_f=\mathbf{k}_S$ since the Cooper-pairs absorbed by the moving SC condensate have momentum $\hbar\mathbf{k}_S$. This leads to a *Doppler shift* $\varepsilon_D=-\hbar^2k_\perp k_S/2m^*$ of the energy of the AR quasiparticle ($k_\perp$ is the transverse wave number).[19] The inset in Fig. 5 illustrates the energy dependence of $|a(\varepsilon)|^2$. The fact that each of the Nb/InAs-banks constitutes *a single* hybrid superconducting terminal is demonstrated by the two BTK-like peaks in the spectrum, one at Δ_{Nb} and another at a smaller energy determined by $\Gamma_{\rm MCM}$. Similar hybrid excitation spectra have recently been observed by scanning tunneling spectroscopy in diffusive Al/Cu-structures.[20] The suppression of $|a(\varepsilon)|^2$ occurs in the range $|\varepsilon|\lesssim\Gamma_{McM}$ when ε_D becomes comparable to the McMillan energy Γ_{McM}.[21]

The solid lines in Fig. 4(a) show $I_{\rm exc}(B)$ obtained from the BTK-model,[4] in which we express the AR amplitude $a(\varepsilon)$ in terms of the McMillan's Green's functions[12,15] accounting for the Doppler shift ε_D in the InAs proximity layer. Using the parameters extracted from Fig. 2, the model reproduces the measured curves quite well (except for the shoulder in $I_{\rm exc}(B_\perp)$, which at present is not understood). The model accounts for the ratio of the $B_\perp$ and $B_\parallel$ scales. This ratio has a simple interpretation if we notice that the relevant value of k_S is related, via the circulation theorem, to the magnetic flux Φ threading the Nb/InAs bilayer for given field orientation [Figs. 4(b) and 4(c)]: $k_S=-\pi/W\times\Phi/\Phi_0$. Neglecting the field inhomogeneity in Nb,[22] we find $\Phi=B_\parallel W(d_S+d_N)$ and $\Phi=B_\perp WW_S$ for the parallel and perpendicular cases, respectively. Consequently, the expected field ratio is $B_\parallel/B_\perp=W_S/(d_S+d_N)=20$, which is within the margins of the experimental uncertainty.

The dramatic reduction in the AR amplitude $a(B)$, inferred from the behavior of $I_{\rm exc}$, can also explain the suppression of the higher lobes of the critical current in the Fraunhofer pattern in weak perpendicular magnetic field [see Fig. 1(d)] since the same $a(B)$ determines the energies of the ABS and hence $I_C(B)$.[12,13] We also note that the smaller the channel width W is, the higher are the values of $B_\perp$ required to reach $\Phi=\Phi_0$ in the junction and the stronger is the suppression of $I_C(B)$ at this point.

Finally, we examined the critical current I_C in a parallel magnetic field for samples No. 1 and No. 2a. Again, even for

the perfectly parallel field there is the phase gradient due to the vector potential [Fig. 4(b)] that induces a Doppler energy shift of the ABS. When it becomes comparable to Γ_{McM}, counterpropagating ABS overlap in energy, and their contributions to I_C gradually cancel. Similar to I_{exc}, the suppression of I_C occurs at ~100 mT. In Fig. 5 we plot $I_C(B)$ for sample No. 1 for several almost parallel field orientations. The small perpendicular component of **B** still leads to a Fraunhofer-like minimum in I_C, which allows a precise determination of the angle α between **B** and the junction plane. This can be described by $I_c(B) = I_c(B_\parallel)|\sin(\pi A B_\perp/\Phi_0)/(\pi A B_\perp/\Phi_0)|$, where $B_\perp = B \sin\alpha$, $B_\parallel = B\cos\alpha$, and A is the junction area. Unlike the standard Fraunhofer pattern,[11] we take into account the dependence of the critical current $I_c(B_\parallel)$ on the parallel component of the field. This is done by straightforwardly generalizing the ballistic formula for the Josephson current,[12] in which we express the AR amplitude a in terms of the McMillan's Green's functions with the Doppler shift in the InAs proximity layers. The dependence $I_c(B_\parallel)$ makes the Fraunhofer-like oscillations decay much faster than the usual $1/B_\perp$ law, which is clearly seen in Fig. 5. For $\alpha \leq 1.3°$ no minimum is detected, while it is still observed for a wider sample No, 2a on the same chip (not shown). The curve for $\alpha \approx 0$ resulted from a careful maximization of I_C at fixed field, since in this case, evidently, no Fraunhofer minimum can be observed anymore. The fits (solid lines in Fig. 5) are obtained by varying the effective thickness of the Nb/InAs bilayer, d_{eff}. We find $d_{\text{eff}} = d_N + d_S = 50$ nm for sample No. 2a (not shown) in agreement with the geometry, while for sample No. 1 $d_{\text{eff}} \approx 25$ nm. The reason for this discrepancy is unclear, since the excess current data in Fig. 4 agree very well. The deviation of the data for $\alpha \approx 0$ from the theoretical $B_\perp = 0$ curve is probably due to a weak perpendicular stray field of the Nb electrodes.

In conclusion, we have studied the IV characteristics and critical current of ballistic Nb/InAs Josephson junctions in parallel and perpendicular magnetic fields. The observed field dependence is much stronger than anticipated from standard models and can be traced back to the Doppler shift of Andreev levels due to diamagnetic supercurrents in hybrid Nb/InAs contacts. Several different aspects of the proximity effect are consistently and nearly quantitatively described by our theoretical model.

We thank J. C. Cuevas and N. Shchelkachev for helpful discussions. The work was supported by the DFG (STR 438-2 and GRK 638) and partially by MPI-PKS (G.T.).

*Present address: Institute for Theoretical Physics and Astrophysics, University of Würzburg, Germany.

[1] I. O. Kulik, Zh. Eksp. Teor. Fiz. **57**, 1745 (1969) [Sov. Phys. JETP **30**, 944 (1970)].

[2] For a review see, e.g., T. Schäpers, *Superconductor/Semiconductor Junctions* (Springer, Berlin, 2001), and the references therein.

[3] P. E. Gregers-Hansen, E. Hendricks, M. T. Levinsen, and G. R. Pickett, Phys. Rev. Lett. **31**, 524 (1973); T. M. Klapwijk, G. E. Blonder, and M. Tinkham, Physica B & C **109–110**, 1657 (1982).

[4] G. E. Blonder, M. Tinkham, and T. M. Klapwijk, Phys. Rev. B **25**, 4515 (1982).

[5] C. Nguyen, H. Kroemer, and E. L. Hu, Phys. Rev. Lett. **69**, 2847 (1992); H. Takayanagi, T. Akazaki, and J. Nitta, *ibid.* **75**, 3533 (1995); J. P. Heida, B. J. van Wees, T. M. Klapwijk, and G. Borghs, Phys. Rev. B **60**, 13135 (1999); K. Neurohr, Th. Schäpers, J. Malindretos, S. Lachenmann, A. I. Braginski, H. Lüth, M. Behet, G. Borghs, and A. A. Golubov, *ibid.* **59**, 11197 (1999).

[6] H. Hoppe, U. Zülicke, and G. Schön, Phys. Rev. Lett. **84**, 1804 (2000).

[7] J. Eroms, D. Weiss, J. De Boeck, G. Borghs, and U. Zülicke, Phys. Rev. Lett. **95**, 107001 (2005).

[8] I. E. Batov, Th. Schäpers, N. M. Chtchelkatchev, H. Hardtdegen, and A. V. Ustinov, Phys. Rev. B **76**, 115313 (2007).

[9] J. Eroms, M. Tolkiehn, D. Weiss, U. Rössler, J. De Boeck, and S. Borghs, Europhys. Lett. **58**, 569 (2002).

[10] H. B. Heersche, P. Jarillo-Herrero, J. B. Oostinga, L. M. K. Vandersypen, and A. F. Morpurgo, Nature (London) **446**, 56 (2007).

[11] M. Tinkham, *Introduction to Superconductivity* (McGraw-Hill, New York, 1996).

[12] M. Grajcar, M. Ebel, E. Ilichev, R. Kürsten, T. Matsuyama, and U. Merkt, Physica C **372-376**, 27 (2002).

[13] P. W. Brouwer and C. W. J. Beenakker, Chaos, Solitons Fractals **8**, 1249 (1997).

[14] W. L. McMillan, Phys. Rev. **175**, 537 (1968).

[15] A. A. Golubov and M. Yu. Kupriyanov, Physica C **259**, 27 (1996).

[16] P. Samuelsson, A. Ingerman, G. Johansson, E. V. Bezuglyi, V. S. Shumeiko, G. Wendin, R. Kürsten, A. Richter, T. Matsuyama, and U. Merkt, Phys. Rev. B **70**, 212505 (2004).

[17] A. Chrestin, T. Matsuyama, and U. Merkt, Phys. Rev. B **55**, 8457 (1997).

[18] S. Skalski, O. Betbeder-Matibet, and P. R. Weiss, Phys. Rev. **136**, A1500 (1964).

[19] G. Tkachov and K. Richter, Phys. Rev. B **71**, 094517 (2005); G. Tkachov and V. I. Fal'ko, *ibid.* **69**, 092503 (2004).

[20] H. le Sueur, P. Joyez, H. Pothier, C. Urbina, and D. Esteve, Phys. Rev. Lett. **100**, 197002 (2008).

[21] The Zeeman shift ($g_{InAs} = -15$) is 3–4 times smaller than ε_D: I. Zutic and S. Das Sarma, Phys. Rev. B **60**, R16322 (1999).

[22] This is justified, since, for the parallel field, the London penetration depth $\lambda_L \simeq 110$ nm is much larger than half of the Nb/InAs bilayer thickness $(d_S + d_N)/2 = 25$ nm, while, for the perpendicular field, the Pearl penetration depth $\lambda_P = 2\lambda_L^2/d_S \simeq 700$ nm is larger than half of the Nb stripe width $W_S/2 = 500$ mm.